A MEMS Ejector for Printing Applications

A. Gooray (Eastman Kodak Co),
G. Roller (Xerox Corp),
P. Galambos, K. Zavadil, R. Givler, and F. Peter (Sandia National Lab),
J. Crowley (Electrostatic Applications)

Abstract

Ejectors applications range from ink-jet printing to drug delivery. MEMS (Micro-Electro-Mechanical Systems) fabrication techniques, particularly surface micromachining, allow production of small monolithic structures that can be adapted to many applications. We will report on the design, fabrication, and testing of a surface micromachined MEMS liquid ejection system for printing applications.

The ejectors were fabricated using the SUMMiT process (www.sandia.mdl/Micromachine), a surface micromachining process. The only assembly required is electrical connection and attachment of a fluid reservoir. The process includes 3 layers of structural polysilicon (poly), separated by layers of sacrificial silicon dioxide (oxide). The final step of the fabrication process is the removal of the oxide to release the poly structure.

The system ejects small volume (3-4 picoliters), satellite free drops at approximately 10 m/s. To eject a drop a piston is drawn rapidly towards a plate containing a nozzle through which the drop is ejected. The ejectors are electrostatically actuated. Since the electric field is across the ejected fluid, device operation is sensitive to the dielectric strength, breakdown voltage and conductivity of the fluid.

Introduction

MEMS (micro-electro-mechanical systems) fabricated fluid ejection systems have a wide variety of applications ranging from ink jet printing[1] to drug delivery for medical applications.[2] Microfluidic MEMS drop ejectors fabricated using the SUMMiT process accurately control the volume and velocity of fluid dispensed at a very high firing rate. For the drop ejector to function properly, the fluid must be contamination free, compatible with the MEMS components, compatible with the electrostatic requirements and compatible with the materials found within the package. Drop ejectors fabricated from the SUMMiT process consist of five layers of polysilicon separated by layers of sacrificial oxide (SiO_2). The fabricated polysilicon device is "released" by the removal of sacrificial oxide with hydroflouric acid (HF). The drop ejection system operates using an electrostatically driven piston supported by polysilicon springs. The piston drives fluid through a circular nozzle fabricated on the top polysilicon layer.

Numerical Simulation of the Drop Ejector

Prior to fabrication of the drop ejector, numerical modeling of the drop ejection process was conducted. Several levels of analysis were conducted before building the devices: 1) an initial estimate of field strength requirements for drop ejection and for ink dielectric breakdown indicated that the ejector concept was feasible, 2) a 1-D dynamic model was used to investigate the magnitude of the forces involved, and 3) an axisymmetric finite element model was used to provide detailed information for design, to answer specific design questions (e.g. sidewalls or no sidewalls), and to verify that the device would work. Numerical simulation was used to design the devices before fabrication. Device testing showed excelent correlation with the modeling. This process of early detailed modeling led to a very predictive design.

Operation of the drop ejector was simulated with the finite-element code, GOMA. This analysis software, developed during the past several years at Sandia National Laboratories, possesses the necessary attributes to properly model drop creation by the ejector, viz., fluid-solid interaction at the moving piston boundary and implementation of an ALE (Arbitrary Lagrangian-Eulerian) technique to move the mesh in the deforming domain. Field equations (Navier-Stokes in the fluid and finite elasticity in the solid regions) are solved with the Galerkin finite element method using a full-Newton iterative scheme. These techniques, in conjunction with a semi-automated remeshing/remapping procedure allow one to follow drop evolution to the "break-off" point - and in some cases beyond. The remeshing/remapping schemes are needed when the grid becomes sufficiently distorted that accuracy is lost during numerical integration. For the class of problems simulated in this work, usually four or five remeshing steps were needed to advance the simulation to the drop "break-off" point.

The essential features of the drop ejector model are depicted in Figure 1. A thin polysilicon piston (nominally 1-2 µm thick and 50-75 µm in diameter), immersed in a liquid bath, is pulled toward the nozzle cover plate (2-10 µm thick) by a strong, fast-acting electrostatic force which is generated from a voltage difference between the piston and the nozzle cover plate. Hence, the electric field is energized across a liquid layer with the ink acting as a dielectric medium. The result of the piston motion is to force liquid

through the nozzle (15-20 μm diameter), thereby creating a high velocity drop; a portion of the liquid initially found between the piston and the nozzle cover plate is squeezed out radially from beneath the piston and rejoins the fluid in the reservoir during drop ejection. Typically, the initial gap between the piston and the nozzle cover plate ranges from 4-6μm depending upon the particular micromachine design. As the piston is drawn to the nozzle cover plate a linear leaf spring supporting the piston is deflected giving rise to a restoring force which acts to return the piston to its rest position when the activation voltage subsides. Equivalent rate constants, k, for the spring member ranged between 10-50 Kdynes/cm.

Operating features of the ejector and constraints on the ink flow manifest themselves in the numerical model in the form of boundary conditions. The electrostatic force divided by its area of application can be defined as an electrostatic pressure, p, and represented by the expression,

$$p_e = -1/2\ \kappa\varepsilon_0 E^2 \qquad (1)$$

where ε_0 is a constant = 8.85x10^{-7}dynes/volts2, κ is the dielectric constant for the ink, E is the electric field strength. The traction given by Eq. (1) is applied to the leading surface of the piston as shown in Figure 1. The analysis is conducted with a constant field strength driving force resulting in a constant applied electrostatic pressure. Note that the electrostatic pressure is applied only to a portion of the piston surface (that portion of the piston that overlaps the nozzle cover plate); we have neglected the effects from fringe fields. Electrostatic activation of the piston typically lasts for several microseconds.

In a similar manner, the restoring force generated by the leaf spring f_{sp} can be written as,

$$f_{sp} = -k\,(z - z_0) \qquad (2)$$

where the deflection z- z_0 is measured from the initial rest position, z_0, of the piston. This force is applied to a few elements on the backside of the piston. Ink flows freely across the two clearly-marked open-flow boundaries and sticks to all no-slip surfaces (piston, nozzle cover plate and spring mount wall). A symmetry condition is applied to the edge of the model along r=0 which asserts that no normal components of the velocity (fluid) or displacement (solid) can occur along this edge. Finally, a kinematic condition is applied to the mesh at the nozzle to ensure that mass conservation is preserved across this free boundary.

The insert of Figure 1 illustrates the results from a typical drop ejector simulation - this snapshot of a developing drop was taken 15 μsec after electrostatic activation with a piston diameter of 56 μm, peak electric field of 25V/μm, spring rate of 10 Kdynes/cm and field dwell time (piston travel time) of 4.4 μsecs. From the illustration one can see the form of the emerging drop; the ejected mass possesses a bulb-like head with a tapered tail. The total drop volume (head + tail), V_{drop}, was calculated to be 2.5 pl and the average speed of the drop bulb was 4.5 m/sec. The peak pressure, P_{atm}, developed by the ejector for this case (stagnation pressure under the piston) was 3.1 atm. The piston does not make material contact with the nozzle cover plate during field activation because of the relatively large viscous forces that arise when attempting to bring two parallel surfaces together. This squeeze flow resistance works to our advantage in providing electrical isolation during the forward stroke but hinders the return stroke by the opposite mechanism.

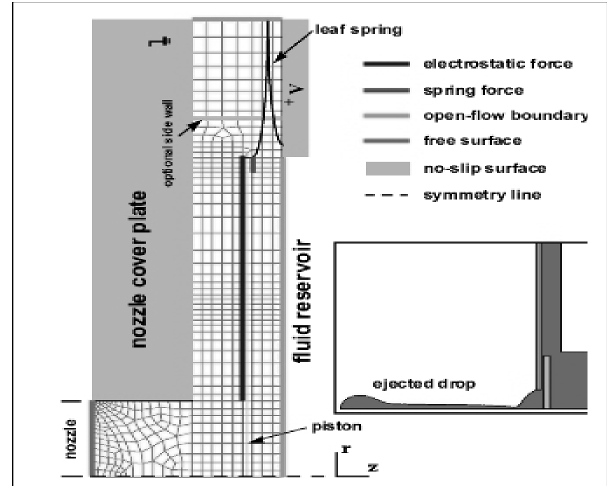

Figure 1. Axisymmetric finite-element model of the drop ejector.

The drop for the "baseline" case was produced with a piston stroke of 3.6 μm. This information can be used to compute an efficiency rating, ζ, for the drop ejector, viz.,

$$\zeta = V_{drop} / V_{disp} \qquad (3)$$

where V_{disp} is the volume of ink displaced by the piston. Eq. (3) indicates that only 28% of the ink displaced by the piston is ejected through the nozzle. The remainder of the displaced ink is squeezed radially outward from beneath the piston and does not contribute to drop formation. In an effort to circumvent this loss, it was decided to surround the piston with a flow confining wall (see Figure 1); the intent of this design modification was to increase ejector efficiency. While the presence of such a side wall did improve the ejector efficiency, its introduction had deleterious effects on ejector performance; Table 1 summarizes ejector performance with changes in side wall position, clearance *gap*.

Table 1. Ejector Performance with a Confining Side Wall

Gap (μm)	P_{max}	drop vel (m/s)	Piston vel (m/s)	Stroke (μm)
infinity	5.3	6.5	2.8	3.9
5	3.2	6.1	2.4	3.5
2	0.9	5.0	1.0	2.0

The parameter used to differentiate between the cases in Table 1 was the clearance gap, defined as the distance between the piston edge and the confining side wall. The data clearly indicate that the presence of a side wall introduces additional flow resistance around the piston and, thereby, degrades both piston and drop velocities when a given power is supplied to the piston (60V for 2.5 µsec). Furthermore, the data in Table 1 indicates that the piston stroke is diminished as the side-wall gap decreases. Surprisingly the drop volume does not seem to be affected by the decrease in piston stroke. We surmise that this effect is offset by the increase in ejector efficiency produced by the presence of the side wall. It does appear that the effect of the side wall begins to diminish (drop & piston velocities recover) as the wall is positioned greater than 5 µm from the piston edge. Because we maintained an interest in producing high-speed drops we decided not to pursue the implementation of an optional side wall for our ejector design.

The performance of the drop ejector can be improved by increasing piston stroke. Figure 2 illustrates the improvement in both drop velocity and size when the initial distance between the piston and the nozzle cover plate is increased from 4.5 to 5.5 µm. Because of the inherent limitations with the surface micromachining process, it is difficult to build structures which offer a piston stroke greater than 5.5 µm. Hence, this value represents an upper bound on current MEMS-based fabrication techniques. Color fringe patterns demarcate the velocity distribution within the drop - units of velocity corresponding to the color legend are cm/s. The maximum velocity within the elongated drop occurs at the base of the bulb where the liquid pressure is low because of the concave curvature of the drop surface. A schematic of the ejector model is shown in the upper left corner of Figure 2.

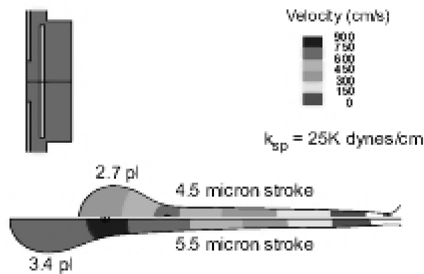

Figure 2. Comparison of drop size and velocity for the ink ejector with a micron of additional stroke. E field is 25 V/micron for a duration of 4.4 microseconds.

Another parameter that was demonstrated to have a profound effect on the performance of the drop ejector is the stiffness of the restoring springs. This is especially significant during the refill stage since the leaf springs are solely responsible for returning the piston to its "ready" position for the next drop cycle. We can summarize the numerical analyses obtained with the following comments: (i) In general, stiffer springs lead to shorter recovery times for the menisci. (ii) Drop size is mostly unaffected by spring stiffness provided the electrostatic pressure dominates the spring force. (iii) It is probably not efficient to wait until the meniscus fully recovers before initiating the next ejector cycle. Much time is consumed in waiting for the meniscus to recover to a completely flat profile. In fact, the driving forces (spring force and pressure gradients generated by the meniscus curvature) that govern the final moments of meniscus recovery become exceedingly small. Thus, to achieve high drop production rates the next drop cycle should start before the meniscus is fully recovered. Judging from the recovery times the model predicts that the drop ejector could be cycled at the following operating frequencies: 10KHz (k = 10K dynes/cm) or 20KHz (k = 50K dynes/cm).

Electric Design of Drop Ejector

Electric Field

The crucial requirement for a MEMS-based ink jet printer is the ability to eject a droplet using the pressure generated by the electric field in the device. While the exact magnitude of the electrostatic pressure depends on details of construction, the magnitude of the pressure at any location in a fluid is given quite simply by Eq. (1).

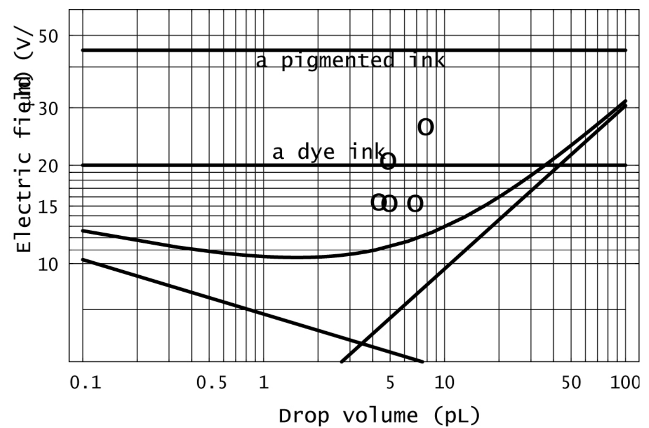

Figure 3. Electric Field needed to overcome mechanical Forces in droplet ejection.

This pressure is opposed by surface tension, the inertia of the fluid and piston, and the viscous drag induced by the motion of the ink in the confined region of the piston and orifice. An estimate of the electric field strength needed to overcome the various mechanical forces for a typical ink jet printer is shown in Figure 3. The figure shows the field requirement as a function of drop size for each opposing force, and for the sum of all the forces. The total field requirement reaches a minimum drop diameter in the range from 10 to 20 µm, which corresponds to a volume of a few pL. The lowest field needed for this example is approximately 10 V/µm, and of course it may become

higher under other circumstances. Fields this large pose some an number of difficulties in the design of the ejector and its driving circuits. The most important ones are electrical breakdown, electrolysis, heating of the ink and driving voltage waveform shaping.

Electric Breakdown

The most fundamental problem is electric breakdown of the ink. The literature value for the break-down of water is approximately 15 V/μm, only slightly above the requirement of Figure 3.

Thus, it is required that the ink withstand the required high field necessary for drop ejection. An empirically-determined, practical field limit for H_2O breakdown in macroscopic gaps (> 1 mm) for ≤ 1 μs potential pulses is nominally 30 $V\cdot\mu m^{-1}$ (3). Srebrov et al. demonstrated a higher breakdown field for H_2O that increased from 40 to 80 $V\cdot\mu m^{-1}$ for a decreasing gap distance of 8 to 1 μm using 5 μs pulses (4). Our computational simulation and prototype device testing show the required field for drop ejection is in the 20 to 30 $V\cdot\mu m^{-1}$ range for an aqueous fluid, so dielectric breakdown is not expected in our ejectors. We confirm this expected absence of breakdown as shown in the data of Figure 4 for a typical candidate aqueous ink. These measurements were made using modules that had a sufficiently short spring to produce a rigid piston. Two different gap dimensions where produced by creating the piston in either the first of the second poly-silicon layer. We find that fields of 70 and 170 $V\cdot\mu m^{-1}$ are stable for 2 μs for 4.5 and 2 μm gaps, respectively. De-ionized H_2O produces similar results with the exception of measurable attenuation of the pulse generator output due to increased current draw. This greater apparent stability at high field is most likely the result of limited charge transport through the native oxide on the poly-silicon surfaces.

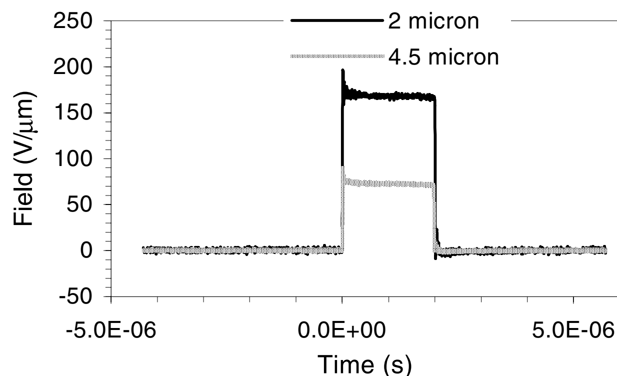

Figure 4. Application of a stable field across aqueous ink-filled ejectors possessing either a 2 or a 4.5 μm gap.

Electrolysis

A second issue of concern is the potential for electrolysis and gas bubble production in these ejectors. Electrolysis sets design limitations on the ejector. Since this ejector applied the electric field inside the ink itself, it raises the possibility that electrochemical reactions will occur at the interface between the electrodes and the liquid. These reactions normally occur when the electric potential exceeds a few volts, and can lead to the production of gases. The drive circuit was designed to prevent the formation of gas bubbles. Since the reactions are basically reversible, we used an alternating pulse train of voltage on the electrode, switching between positive and negative in less that a microsecond. The alternation of voltage ensured that the electrochemical reactions were reversed, and gave no net gas production.

Electrochemistry at the piston and nozzle plate surfaces results in power dissipation and decreases the device efficiency. Gas bubble formation, due to electrolysis, can produce cavitation during bubble nucleation that can be destructive to the piston. In addition, bubbles represent a more compressible fluid further decreasing device efficiency and impeding fluid transport. Measurable current does flow when a high field is applied across the ejector. We measure current densities on the order of 10^2 $A\cdot cm^{-2}$ for de-ionized H_2O at 100 V. Visible O_2 and/or H_2 bubbles start to appear at 300 $A\cdot cm^{-2}$. This current is a quazi-steady state faradaic current that is due to electrolysis of H_2O as a result of large interfacial potential drops. A field of 22 $V\cdot\mu m^{-1}$ requires a potential of 100 V for a 4.5 μm initial inter-electrode gap distances. Even at the intrinsic conductivity of H_2O, a significant fraction of this potential will appear across the $Si/SiO_x/H_2O$ interface allowing for the reduction and oxidation of H_2O at the opposing electrode surfaces. The use of a bi-polar pulse train can aid in minimizing the electrolysis rate. The bi-polar pulse allows for a fraction of the gas generated at one potential extreme to be reduced or oxidized at the other potential extreme. The efficiency for this conversion will depend on relative reaction kinetics and diffusion rates. Tailoring the ink composition can reduce electrolysis rates. The addition of 10 weight percent of ethylene glycol and diethylene glycol, desirable ink additives, decreases this current density by $10^{1.5}$, sufficiently lowering it below an apparent bubble nucleation threshold. It is likely that these diols form surface complexes that limit electron transport to and from H_2O.

We find evidence of oxide growth in our ejectors as manifest in a significant decrease in device current with repetitive pulsing at 100 V using de-ionized water. This effect is less pronounced with diol-H_2O mixtures and inks. Minimizing an individual pulse width (i.e. 200 ns) is expected to reduce the effects of oxide growth because of the limited mobility of the OH^- anion in the oxide.[5]

Heating of the Ink

A second design challenge with fields this high is Joule heating of the liquid during the ejection pulse. The electric power density in the fluid is given by

$$P = E^2/\rho \quad (4)$$

where ρ is the electrical resistivity of the ink. With water-based inks, the resistivity can be quite low, leading to rapid

heating of the ink during ejection. The time needed to raise the ink by a given temperature can be estimated from the thermal balance equations, and is shown in Figure 5. As expected, less time is allowed when the field is high, or when the ink resistivity is low. In practice, this has required a different ink formulation from that normally used in ink-jet printers.

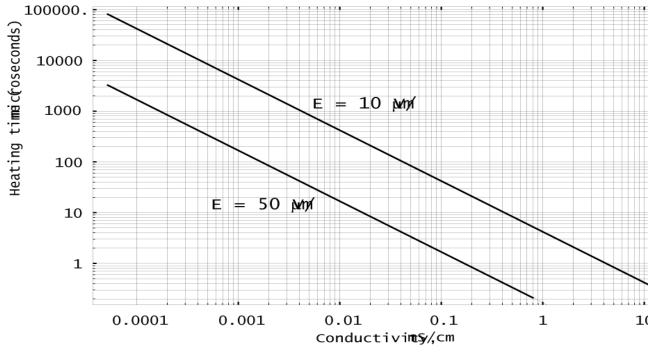

Figure 5. Time required to raise temperature of ink

Driving Voltage

The piston is moving during the ejection pulse, so that the gap decreases from its initial value of 5µm to a much smaller value on the order of 1 - 2µm. If the drive is set up to provide an electric field close to the breakdown strength at the beginning of the ejection cycle, it will supply a much stronger field at the end unless the voltage is reduced. Reduction of the voltage during piston closing can be achieved by a number of methods, including driving the piston with a current source or tailoring the voltage pulse train to decay during the cycle. The latter method was used in the device described here, with the voltage decay selected from modeling results for the piston motion during the cycle.

MEMS Ejector Design and Fabrication

The ejector array was designed for and fabricated in the SUMMiT process (www.mdl.sandia.gov/Micromachine). This fabrication process is a batch MEMS process that can be adapted to inexpensive mass production (similar to Integrated Circuit, IC, fabrication). It is currently used as a prototyping process. Up to eight different prototype design modules are incorporated on a silicon wafer. A lot of wafers (typically 6-10 wafers per lot) is fabricated using standard IC fabrication tools adapted for MEMS. The prototype designs can then be tested. The SUMMiT process is a surface micromachining process that utilizes polysilicon (poly) as the structural material and silicon dioxide (sacox) as the sacrificial material. The current SUMMiT process has 5 levels of poly (Fig. 6). Structural and sacrificial layers alternate in a stack of thin films on top of a silicon wafer. Cuts in the sacox layers allow connection between poly layers for anchoring structures and making electrical connections. The final step in the fabrication process is the release etch. An HF/HCl acid bath removes the sacox layers, leaving the polysilicon structure behind. The bottom layer is a thermally grown oxide capped by silicon nitride, and provides electrical isolation between the MEMS devices and the silicon substrate.

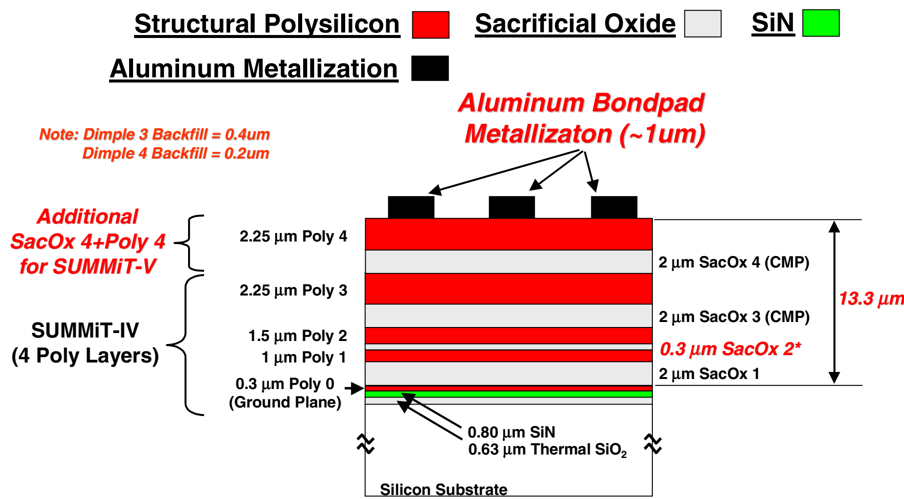

Figure 6. SUMMiT Layer Stack. Five layers of polysilicon (poly) alternate with 4 layers of sacrificial silicon dioxide (sacox). The bottom layer of poly is used for electrical connections and the top 4 layers for MEMS structures. The first layer of thermal oxide covered with silicon nitride provides electrical isolation from the silicon substrate.

The ejectors were designed using AutoCAD (ACAD). A top view of the ACAD drawing is shown in Fig. 7. Each different color is a different drawing layer. One or more drawing layers are needed to create a mask. Each mask is used to photolithographically pattern photoresist on top of a deposited layer of poly or sacox. Therefore the mask layers define the polysilicon layer shapes that make up the device structure. Sandia National Laboratories has incorporated cross-sectional visualization and three-dimensional (3D) visualization software into ACAD2000. The visualization software is used to simulate the fabrication process. Process information pertaining to thin film thickness and etching characteristics is incorporated into the software. The visualization tools allow one to accurately predict what the MEMS structure will look like before fabrication. These tools are especially important because the batch fabrication process requires about 4 months to complete. A 3D visualization of a single ejector piston is shown in Fig. 8. The piston is approximately 50 microns square and is supported on two sides by springs. The stroke length of the piston is approximately 5 microns.

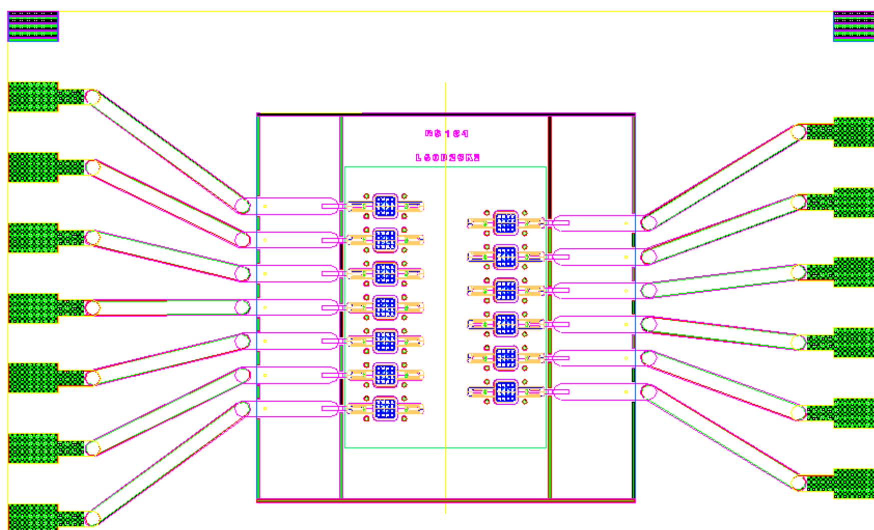

Figure 7. AutoCAD design of ejector array. Ejectors (13 in each array) are individually addressable from 13 different bond pads. Ejector pistons supported on two sides by springs.

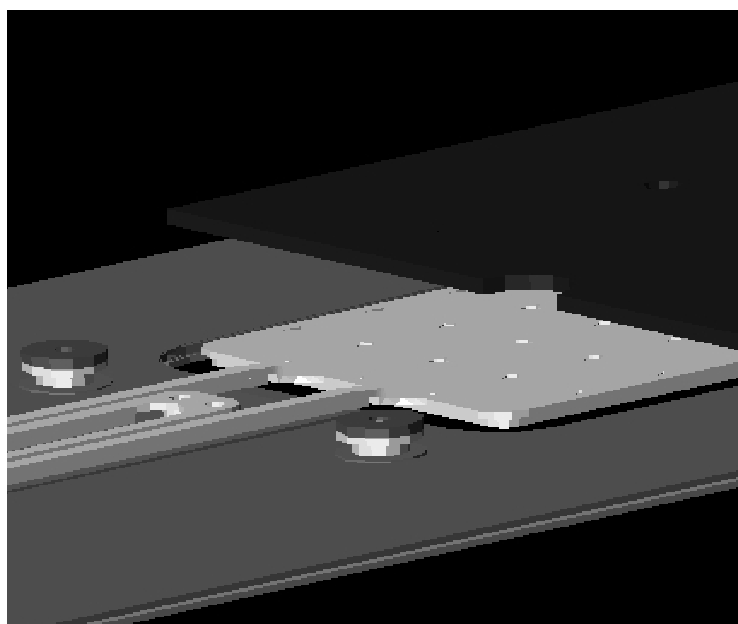

Figure 8. 3D Visualization of Single Ejector. One half of the nozzle cover plate (blue – poly3) is cut away to reveal the piston beneath. The piston (gray – poly1) sits in a well created by the nitride cut and is supported by springs on two sides. One of the springs is shown and continues beyond the left edge of the figure. Support posts (red top – poly2) stiffen the nozzle cover plate.

An SEM of the as-fabricated ejector array is shown in Fig. 9. The top cover containing the ejection nozzles has been torn away in this view to reveal the piston structure beneath. The 'waffle iron' pattern on the pistons is due to the dimple cut that was used to stiffen the piston. A dimple cut consists of cuts that only go part way through the oxide instead of entirely through the oxide as an anchor cut would. The next layer of the poly (poly1 - the piston) is deposited on the underlying oxide (sacox1 in this case). The conformal deposition process accounts for the 'waffle iron' pattern. The grooves in the piston are at the dimple cut stiffener locations. The grooves do not show up in the visualization (Fig. 8) because an idealized vertical wall deposition process is assumed in the simulation software. Otherwise the simulation accurately reflects the as-built SEM (Fig. 9). In particular, the nitride cut around the piston that causes the piston to sit in a hole is shown in both figures.

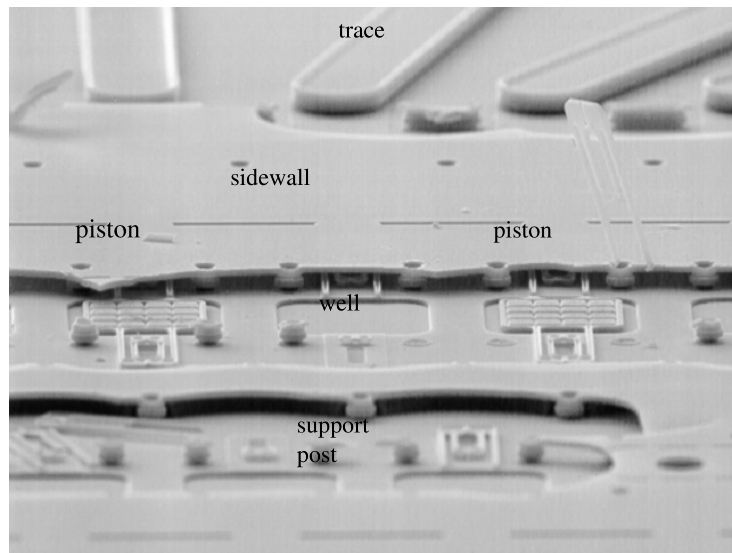

Figure 9. SEM of Ejector Array. Part of the nozzle cover plate has been torn away to reveal the pistons beneath. Some of the pistons are also removed. No Bosch etch has been performed. The well created by the nitride cut is clearly visible as is the 'waffle iron' pattern on each piston and piston support springs.

The nitride cut is used to remove the nitride and oxide layers form the area directly beneath each piston. A Bosch etch process (Bosch. Patent No. 5501893: *Method of Anisotropically Etching Silicon,* Robert Bosch Gmbt, Issued 1996) is used to cut a vertical walled via from the back of the wafer to the front behind each piston. The Bosch etch is highly selective to silicon and stops on the first layer of oxide it encounters. In this case, the nitride cut ensures that the Bosch etch stops on sacox1 underneath the piston. A two step Bosch process was used to provide a common ink reservoir and because the aspect ratio for a full wafer etch of a 50 micron square hole is too large to effectively etch in one step (the pistons are approximately 50 microns square). After the Bosch etch is complete the wafers are diced to ejector array size and packaged. The prototype ejector arrays are then ready for packaging and testing testing. A typical packaging design is shown in Fig. 10.

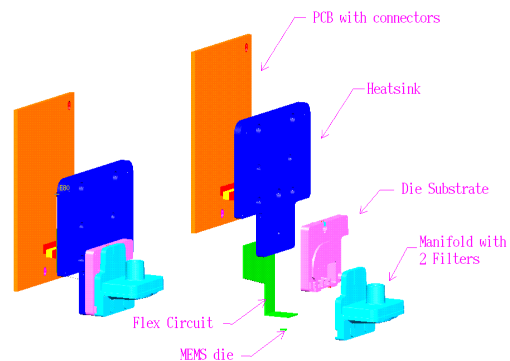

Figure 10. Print Head Packaging Design

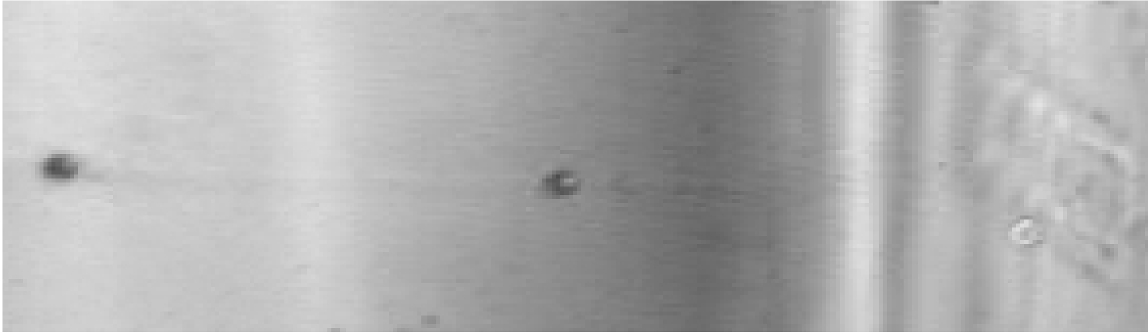

Figure 11. Image of Ejected Drops

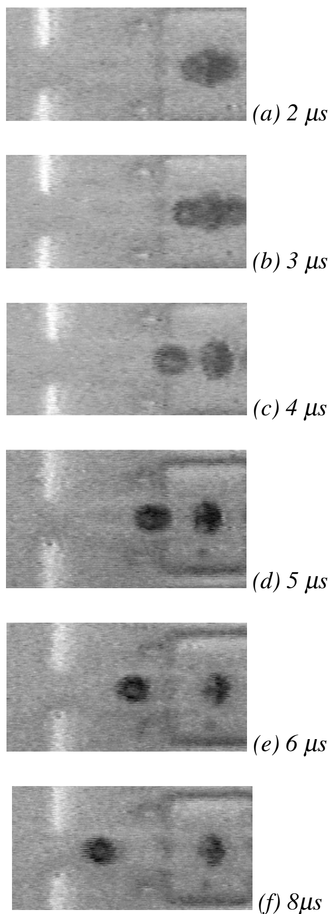

Figure 12. Drop Formation and Ejection time

Results and Conclusions

The ejector testing procedures are described in a previous publication by the authors.[6] The voltage signal sent to the ejector is a bi-polar constant field signal. The peak voltage is adjustable, depending on the ink properties, and can be as large as 100 V. Parameters measured are drop velocity, drop volume, directionality and firing frequency. Inks ejected are typical TIJ aqueous based inks. With an ES device, it is important for the ink to have a large as possible di-electric and small as possible conductivity. For these inks di-electric is about 70 and conductivity 0.001 S/m. Typical results obtained are shown in Table 2.

Table 2. Performance of ES Drop Ejector

Parameters	ES Ejector
Piston Size	60 x 60 μm
Drop Generation Height	4.5 microns
Nozzle Diameter	20 μm
Drop Volume	4 pico liters
Volumetric Efficiency	38%
Drop Velocity	9.5 m/s
Reset Time	13 μs
Drop Rate, K Colors	10 kHz (active pull down & stiffer spring will increase this)
Energy to eject a drop ε & σ dependent, ε =68, σ = 0.001 S/M	<0.003 μJ/pl

This paper describes a novel IJ drop ejector design. The design is fully predictive and parts manufactured utilized a very mature monolithic process. The first design resulted with very good drop ejection of real inks.

References

1. R. R. Allen, J. D. Meyer, W. R. Knight, "Thermodynamics and Hydrodynamics of Thermal Ink Jets", *Hewlett Packard Journal,* May 1985.
2. B. De Heij, G. van der Schoot, B. Hu, J. Hess, N. F. de Rooij, "Characterization of Fluid Droplet Generator for Inhalation Drug Therapy", *Sensors and Actuators A* **85** (2000), pp. 430-434.

3. H.M. Jones and E.E. Kunhardt, Pulsed Dielectric Breakdown of Pressurized Water and Salt Solutions**,** *J. Appl. Phys.* **77(2),** 1995, 795-805.
4. B.A. Srebrov, L.P. Dishkova and F.I. Kuzmanova, *Electrical Breakdown of a Small Gap Filled with Distilled Water*, *Sov. Tech. Phys. Lett.* **16(1),** 1990**,** 70-71
5. K. Ghowsi and R.J. Gale, Theoretical Model of the Anodic Oxidation Growth Kinetics of Si at Constant Volatge, *J. Electrochem. Soc.* 136**(3),** 1989,867-871.
6. P. Galambos, et al., A Surface Micromachine Electrostatic Drop Ejector, *11th International Conference on Solid- State Sensors and Actuators*, Munich, Germany, June 2001.